Peer-reviewed version available at Water 2020, 12, 337; doi:10.3390/w12020337

Newton's Shear Flow Applied to Infiltration and Drainage in Permeable Media

Peter F. Germann, Prof. em. University of Bern, Switzerland, pf.germann@bluewin.ch

Abstract

The paper argues that universal approaches to infiltration and drainage in permeable media that pivot around capillarity and that led to dual porosity, non-equilibrium, or preferential flow need to be replaced by a dual process approach. One process has to account for relatively fast infiltration and drainage based on Newton's shear flow, while the other one is responsible for storage and relatively slow redistribution of soil water by focusing on capillarity. Already Schumacher (1864) postulated two separate processes. However, Buckingham's (1907) and Richards' (1931) apparent universal capillary-based approach to flow and storage of water in soils dominated. The paper introduces the basics of Newton's shear flow in permeable media. It presents experimental support for the four presumptions of (i) sharp wetting shock fronts; (ii) that move with constant velocities; (iii) atmospheric pressure prevails behind the wetting shock front; (iv) laminar flow. It further discusses the scale tolerance of the approach, its relationship to Darcy's (1856) law, and its extension to solute transport.

Key words

Wetting shock fronts, shear flow, viscosity, capillarity, kinematic waves.

Introduction

Infiltration is the transgression of liquid water from above the surface of the permeable lithosphere to its interior, while drainage refers to liquid water leaving some of its bulk. Infiltration and drainage still bear unsolved problems. For instance, Blöschl et al. (2019), in a most thorough, exhaustive, and detailed survey among hundreds of active hydrologists, compiled 23 Unsolved Problems in Hydrology (UPHs). The 7th UPH asks "Why is most flow [in the unsaturated lithosphere P.G.] preferential across multiple scales and how does such behaviour co-evolve with the critical zone?" The critical zone in hydrology delineates the upper most layer of the lithosphere that is in direct contact with the atmosphere. It typically carries the terrestrial ecosystems and thus simultaneously provides water, air, nutrients, and mechanical support to roots of most terrestrial plant communities. In general, the critical zone is congruent with soil. This contribution presents a solution of the 7th UPH.

The second section reviews the evolution of infiltration concepts in partially saturated soils since the second half of the 19th century. The next one summarizes Newton's shear flow applied to flow in permeable media, while the other ones provide support to, and various applications of the approach.

Review of infiltration concepts

In the mid-19th century, there was an increasing interest in flows in saturated soils and similarly permeable media. Hagen, a German hydraulic engineer, and Poiseuille (1846), a French physiologist, independently analyzed laminar flow in thin capillary tubes. Darcy (1856), in the quest of designing a filtration system for the city of Dijon, empirically developed the concept of hydraulic conductivity as proportionality factor of flow's linear dependence on the pressure

gradient. Dupuit (1863) expanded Darcy's law to two dimensions as perpendicular and radial flow between two parallel drainage ditches and towards a groundwater well, respectively.

Schumacher (1864), a German agronomist, was probably the first who considered capillarity as the cause for simultaneous flows of water and gas in partially water-saturated soils. He qualitatively compared the rise of wetting fronts in soil columns with the rise of water in capillary-sized glass tubes, and concluded that the wetting fronts rise higher but slower in finer textured soils compared with coarser materials. He also infiltrated water in columns of undisturbed soil and found that infiltration fronts progressed much faster than the rising wetting fronts. He suggested two separate processes for the two flow types: (i) slower capillary rise and (ii) faster infiltration, however, without further dwelling on infiltration. Lawes et al.(1882) concluded from the chemical composition of the drain from large lysimeters at the Rothamsted Research Station that "*The drainage water of a soil may thus be of two kinds (1) of rainwater that has passed with but little change in composition down the open channels of the soil; or (2) of the water discharged from the pores of a saturated soil."* Lawes et al. (1882) prioritized two separate flow paths to explain the observations.

During the second half of the 19th century irrigation agriculture spread in semi-arid areas and so increased the demand for better understanding of the soil-water regime. Buckingham (1907), working on an universal approach to the simultaneous storage and flow of water and air in soils, postulated the relationship between the capillary potential ψ (Pa) and the volumetric water content θ (m^3 m^{-3}), also known as the water retention function, retention curve, or water release curve. The capillary potential follows from the Young (1805)-Laplace relationship, stating that the pressure difference between a liquid and the adjacent gas phase increases inversely proportional to the radius of the interface. In addition to the specific weight of the soil water, Buckingham (1907) introduced the spatial gradient of ψ as the other major driving force, thus allowing for the redistribution of soil water in all directions, evaporation across the soil

surface, transpiration via roots, and capillary rise from perched water including groundwater tables. In analogy to Fourier's (1822) and Ohm's (1825) laws for heat flow and electrical current, and Darcy's (1856) law for water flow in saturated porous media, Buckingham (1907) also proposed the hydraulic conductivity for flow in unsaturated porous media as function of either $K(\theta)$ or $K(\psi)$ (m s^{-1}). According to Or (2018), the British meteorologist Richardson (1922) was most likely the first who introduced a diffusion type of K-ψ-θ-relationship in the quest of quantifying water exchange between the atmosphere and the soil as lower boundary of the meteorological system. A second-order partial differential expression became necessary because ψ depends on θ, and both their temporal variations on flow, while flow is driven by the gradient of ψ. The race was on to the experimental determination of the K-ψ-θ-relationships. For instance, Gardner et al. (1922) applied plates and blocks of fired clay with water-saturated pores fine enough to hydraulically connect the capillary bound water within soil samples with systems outside them. Richards(1931) applied the technique to the construction of tensiometers that directly measure ψ within an approximate range of $0 > \psi \gtrsim -80$ kPa ($\psi = 0$ corresponds to the atmospheric pressure as reference). With the pressure plate apparatus he measured ψ-θ-relationships and determined hydraulic conductivity $K(\psi$ or $\theta)$. Similar to Richardson (1922), he presented a diffusion-type approach to the transient water flow in unsaturated soils. Numerous analytical procedures evolved for solving the well-known Richards (1931) equation. Van Genuchten (1980), for instance, developed a closed form of K-ψ-θ-relationships that provide the base for the many hues of HYDRUS, a numerical simulation packages dealing with flow and storage of water and solutes in unsaturated soils (e.g. Simunek et al., 2008).

Veihmeyer (1927) investigated water storage in soils in the quest of scheduling irrigation schemes. He proposed the water contents at the field capacity FC and at the permanent wilting point PWP as upper and lower thresholds of plant-available soil water, where FC gets established a couple of days after a soil was saturated under exclusion of evaporation (also

referred to as 'drainable or gravitational soil water'). Various methods appeared on how to establish PWP that is accepted today at -15 bars. It became unavoidable that concepts based on Buckingham's (1907) fundamental and seminal work contradicted with practical and field-oriented research. Veihmeyer (1954), for instance, stated "Since the distinction between capillary and other 'kinds' of water in soils cannot be made with exactness, obviously a term such as non-capillary porosity cannot be defined precisely since by definition it is determined by the amount of 'capillary' water in the soils".

Progress in field instrumentation and computing techniques allowed for producing and processing large data sets including the numerical solution of Richards' (1931) equation. In the late 1970s, the development increasingly unveiled substantial discrepancies between measurements and the numerous approaches to water movement in unsaturated soils based on Richards' (1931) capillarity-dominated theory. Particularly disturbing were observations on wetting fronts advancing much faster than expected from the Richards approach. Concepts like macropore flow (e.g., Beven and Germann, 1982) and flow at non-equilibrium with respect to the ψ-θ-relationship appeared. Jarvis et al. (2016) summarized as preferential all the flows in unsaturated porous media not obeying Richards' (1931) equation. See also Morbidelli et al. (2018) for a recent review on infiltration approaches. Beven (2018) argued that, for about a century, the hardly questioned preference given to capillarity denied recognition of concepts considering flow along macropores, pipes, and cracks. Indeed, there is an increasing number of contributions focusing on the dimensions and shapes of flow paths, their 3-d imaging, and trials to derive flows from them (e.g., Abu Najm et al., 2019). However, there is hardly an approach capable of applying the wealth of information about the paths to the quantification of flow. Ignoring Veihmeyer's (1954) warning, the attraction of research on flow paths is so dominant that, for instance, Jarvis et al. (2016) flatly denied the applicability of Hagen-Poiseuille concepts to flow in soils. (See Germann, 2017, and Jarvis et al. 2017). Moreover, advanced techniques

of infiltration with non-Newtonian fluids led so far just to the description of path structures rather than more directly to the flow process (Atalah and Abou Najm, 2018). Wide-spread research in the types, dimensions, and shapes of 'macropores' and their apparent relationships to flow and transport mostly pivot around Richards (1931) equation that is numerically applied to either macropore-/ micropore-domains or by modelling flow and transport in the macropore domain with separate rules yet still maintaining a Richards-type approach in the micropores. Both approaches allow for due exchange of flow and transport between the two domains. Imaging procedures visualize flow in 2-d and 3-d in voids as narrow as some 10 µm, rising hope that the wealth of information gained at the hydro-dynamic scale will eventually lead to macroscopic models at the soil profile scale of meters (see, for instance, Jarvis et al., 2016). Thus, Beven's (2018) denial of progress in infiltration research is here carried a step further. The obsession with pores, channels, flow paths, and their connectivity, tortuosity, and necks actually retards research progress towards more general infiltration that should be based on hydro-mechanical principles as the 7th Unresolved Problem in Hydrology demands.

A second thread, leading to the alternative infiltration approach presented here, is traced back to Schumacher's (1864) dual-processes. He suggested that infiltration follows rules, though unspecified at that time, that markedly differ from the capillary rise out of water tables. Moreover, the alternative approach should be based on the same principles as Hagen-Poiseuille's (1846) and Darcy's (1856) laws, thus closing the gap of one to two orders of magnitude of hydraulic conductivity between saturated flow and flow close to saturation (Germann and Beven, 1981a).

In his quest of demonstrating the benefits of forests and reforestations on controlling floods and debris flows from steep catchments in the Swiss Alps and Pre-Alps, Burger (1922) measured in situ the time lapses Δt_{100} for the infiltration of 100 mm of water into soil columns of the same length. In the laboratory, he determined the air capacity AC (m^3 m^{-3}) of undisturbed

samples taken near the infiltration measurements, where *AC* is the difference of the specific water volume after standardized drainage on a gravel bed and complete saturation. Germann and Beven (1981b) found an encouraging coefficient of determination of $r^2 = 0.77$ when correlating via a Hagen-Poiseuille (1846) approach 76 pairs of Δt_{100}- and *AC*-values. Following Lawes et al. (1882), who distinguished between fast and slow drainage, Germann (1986) assessed the arrival times of precipitation fronts in the Coshocton lysimeters. Accordingly, rains of 10 (mm/d) sufficed to initiate or increase drainage flow within 24 hours at the 2.4-m depth if the volumetric water content in the upper 1.0 m of the soil was at or above 0.3 ($m^3\ m^{-3}$). The observations result in wetting front velocities greater than 3×10^{-5} ($m\ s^{-1}$). Beven and Germann (1981) modelled flow in tubes and planar cracks, and proposed kinematic wave theory according to Lighthill and Whitham (1955) as analytical approach to Newton's shear flow. Germann (1985) applied the theory successfully to data from an infiltration-drainage experiment carried out on a block of polyester consolidated coarse sand. The paper is considered a precursor of the following section that treats infiltration and drainage in permeable media as exclusively gravity driven and viscosity controlled, while capillarity may adsorb water from flow to the sessile parts of the system.

Theory

a) Basic relationships

The approach is laid out at the hydro-mechanical scale of spatio-temporal process integration, allowing for its easy handling with analytical expressions, yet under strict observance of the balances of energy, momentum, and mass (i.e., the continuity requirements). The approach builds on four presumptions that are not necessarily common to soil hydrology: (i) infiltrating water forms a sharp wetting shock front; (ii) the wetting shock front moves with constant velocity; (iii) atmospheric pressure prevails in the mobile

Preprints (www.preprints.org) | NOT PEER-REVIEWED | Posted: 13 November 2019 doi:10.20944/preprints201911.0150.v1

Peer-reviewed version available at Water 2020, 12, 337; doi:10.3390/w12020337

water between the wetting shock front and the surface; and (iv) flow is laminar (i.e., Reynolds numbers may not exceed values close to unity).

The interior of a permeable solid medium contains connected flow paths that are wide enough to let liquids pass across the volume considered. The definition purposefully avoids further specification of the flow paths' shapes and dimensions. Water supply to the surface is thought of a pulse $P(q_S, T_B, T_E)$, where q_S (m s^{-1}) is constant volume flux density from the pulse's beginning at T_B to its ending at T_E (both s). (The subscript S refers to the surface of the permeable medium). The pulse initiates a water content wave *WCW* of mobile water that is conceptualized as a film gliding down the paths of a permeable medium according to the rules of Newton's shear flow. The parameters film thickness F (m) and specific contact length L (m m^{-2}) per unit cross-sectional area A (m^2) of the medium specify a *WCW*. Regardless of the thickness of F, atmospheric pressure prevails in the film. Figure 1 illustrates the concept.

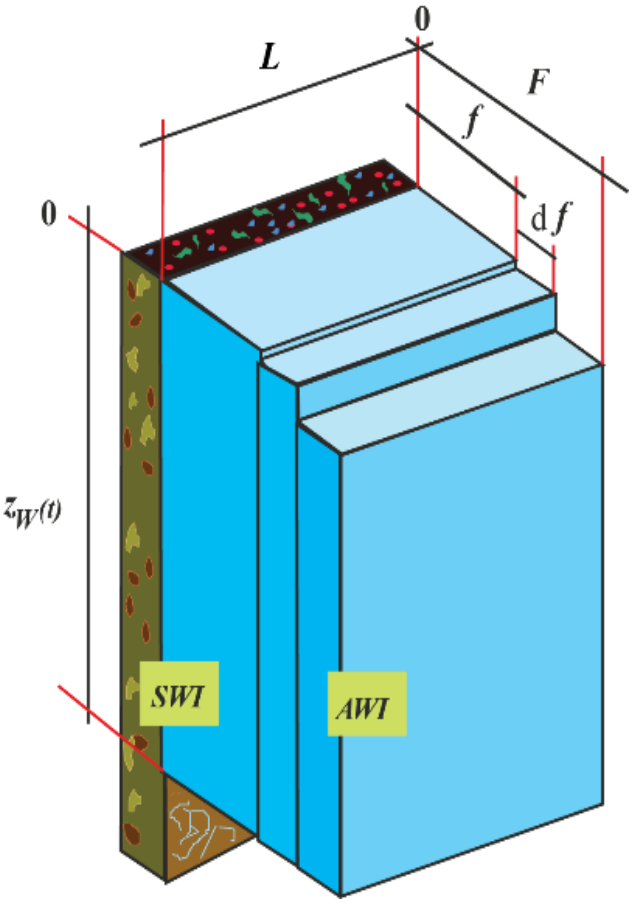

Figure 1: Film flow along a vertical plane, where F (m) is the film thickness, f (m) is the thickness variable, df (m) is the thickness of a lamina, $z_W(t)$ (m) is the vertical position of the wetting shock front as function of time t (s), and L (m m^{-2}) is the specific contact length between the moving water film and the sessile parts of the permeable medium per its unit horizontal cross-sectional area A (m^2). *AWI* and *SWI* are the air-water and the solid-water interfaces, respectively. (From Germann, 2014; with permission from the publisher).

A *WCW* supposedly runs along the flow paths while forming a discontinuous and sharp wetting shock front at $z_W(t)$. The *WCW* partially fills the upper part of the medium within $0 \leq z \leq z_W(t)$ with the mobile water content $w(z,t)$ ($m^3\ m^{-3}$), where $w \leq \varepsilon - \theta_{ante}$ with porosity ε and antecedent soil moisture θ_{ante}, both ($m^3\ m^{-3}$). The lower part $z > z_W(t)$ remains at θ_{ante}. The coordinate z (m) originates at the surface and points positively down.

Newton (1729) introduced viscosity as *"The resistance, arising from the want of lubricity in the parts of a fluid, is,* caeteris paribus*, proportional to the velocity with which the parts of the fluid are separated from each other."* In our case, the definition translates to the shear force in the unit area of L x A x $z_W(t)$ (m^2) per unit volume A x $z_w(t)$ m^3) of the medium at distance f (m) from the *SWI*. Accordingly, L ($m\ m^{-2}$) is not only the specific contact length of the film per A, but L ($m^2\ m^{-3}$) evolves as the specific vertical contact area of the *WCW* with the sessile parts of the permeable medium per unit volume. Thus, the shear force at f amounts to

$$\varphi(f) = -\eta \cdot \rho \cdot \left.\frac{\mathrm{d}v(f)}{\mathrm{d}f}\right|_f \qquad (1)$$

($N\ m^{-2}$), where η ($\approx 10^{-6}\ m^2\ s^{-1}$) is the temperature dependent kinematic viscosity of water, ρ (1000 kg m^{-3}) is the water's density, $v(f)$ ($m\ s^{-1}$) is the velocity of the lamina at f in the vertical-down direction, and $\mathrm{d}v(f)/\mathrm{d}f$ is the velocity gradient in the horizontal direction. The expression ρ x $v(f)$ is the water's momentum at f, while ρ x $\mathrm{d}v(f)/\mathrm{d}f$ is the gradient of momentum causing its dissipation towards the *SWI* while η acts as its dissipation coefficient. Equation [1] holds for incompressible liquids during laminar flow while φ acts in the direction opposite to v. $\varphi(f)$ is considered to balance the weight of the film from f to F such that

$$\rho \cdot g \cdot L \cdot z_W(t) \cdot (F - f) = \eta \cdot \rho \cdot L \cdot z_W(t) \cdot \left.\frac{dv}{df}\right|_f \qquad (2)$$

(N). Integration of Eq.[2] from the *SWI*, where $v(0) = 0$ (the non-slip condition), to f yields the parabolic velocity profile from the SWI to f as

$$v(f) = \frac{g}{\eta} \cdot (F \cdot f - \frac{f^2}{2}) \quad (3)$$

The differential volume flux density at f is

$$dq|_f = L \cdot v(f) \cdot df \quad (4)$$

(m s^{-1}). Its integration from the *SWI* at $f = 0$ to the air-water interface *AWI* at $f = F$ produces the volume flux density of the film as

$$q(F,L) = \frac{g}{3 \cdot \eta} \cdot L \cdot F^3 \quad (5)$$

(m^3 s^{-1}), while the volume of mobile water per unit volume of the permeable medium from the surface to $z_W(t)$ amounts to

$$w(F,L) = F \cdot L \quad (6)$$

(m^3 m^{-3}). The constant velocity of the wetting shock front follows from the volume balance amounting to

$$v_W(F) = \frac{q(F,L)}{w(F,L)} = \frac{g}{3 \cdot \eta} \cdot F^2 \quad (7)$$

while the position of the wetting shock front as function of time becomes

$$z_W(t) = v_W \cdot (t - T_B) = (t - T_B) \cdot \frac{g}{3 \cdot \eta} \cdot F^2 \quad (8)$$

The terms relating to velocity depend exclusively on F^2, Eqs.[3, 7, 8], while those relating to mobile water and its volume flux density also on L, Eqs. [5, 6].

Under consideration of $z_W(t)$, L expresses the specific vertical contact area of the *WCW* per unit volume of the permeable medium as the locus where momentum, heat, capillary potential, water, solutes, and particles get exchanged between the *WCW* and the sessile parts of the medium.

Equations [3 to 8] hold during infiltration i.e., $T_B \leq t \leq T_E$. Input ends abruptly at T_E and at $z = 0$ i.e., $q_S \rightarrow 0$, when and where the *WCW* collapses from $f = F$ to $f = 0$. All the rear ends

of the laminae are released at once at $z = 0$. They move downwards with $v(f)$ according to Eq. [3]. The outermost lamina moves the fastest with the celerity of the draining front as

$$c_D = \frac{\mathrm{d}q(F)}{\mathrm{d}w} = \frac{\mathrm{d}q(F)}{L \cdot \mathrm{d}f} = \frac{g}{\eta} \cdot F^2 = 3 \cdot v_W \tag{9}$$

Celerity refers to the velocity of a flow property change. The slower moving wetting front intercepts the faster draining front at time T_I (s), that follows from setting v_W x (T_I-T_B) = c_D x (T_I-T_E), as

$$T_I = \frac{1}{2} \cdot (3 \cdot T_E - T_B) \tag{10}$$

Thus, T_I is an exclusive expression of the pulse duration. The wetting front intercepts the draining front at depth

$$Z_I = (T_E - T_B) \cdot F^2 \cdot \frac{g}{2 \cdot \eta} \tag{11}$$

The rear ends of all the other laminae move with decreased celerities. According to Eq. [9], the celerity c_{RE} (f) of the rear end of a lamina between $0 < f < F$ is

$$c_{RE}(f) = \frac{\mathrm{d}q(f)}{\mathrm{d}w} = \frac{\mathrm{d}q(f)}{L \cdot \mathrm{d}f} = \frac{g}{\eta} \cdot f^2 = \frac{z_{RE}(f)}{t - T_E} \tag{12}$$

Rearranging the last two terms in Eq. [12] and solving for f leads to the temporal position of the film thickness as

$$F_{RE}(z,t) = \left(\frac{\eta}{g}\right)^{1/2} \cdot z^{1/2} \cdot (t - T_E)^{-1/2} \tag{13}$$

Multiplication of $F_{RE}(z,t)$ with L leads to the spatio-temporal mobile water content of the *WCW* as trailing wave according to

$$w(z,t) = L \cdot \left(\frac{\eta}{g}\right)^{1/2} \cdot z^{1/2} \cdot (t - T_E)^{-1/2} \tag{14}$$

Preprints (www.preprints.org) | NOT PEER-REVIEWED | Posted: 13 November 2019 doi:10.20944/preprints201911.0150.v1

Peer-reviewed version available at Water 2020, 12, 337; doi:10.3390/w12020337

After T_I and beyond Z_I the draining front disappears and $v_W(z,t)$ decreases with time and depth. However, the shape of the *WCW* remains according to Eq. [14] over the depth range of $0 \le z \le z_W(t)$. The volume balance of the *WCW* amounts to

$$q \cdot (T_E - T_B) = V_{WCW} = \left(\frac{\eta}{g}\right)^{1/2} \cdot L \cdot (t - T_E)^{-1/2} \cdot \int_0^{z_W(t)} z^{1/2}\, dz \tag{15}$$

where V_{WCW} (m) represents the water volume of the *WCW* that has infiltrated during T_E-T_B. Solving Eq.[15] for $z_W(t)$ leads to the temporal position of the wetting shock front as

$$z_W(t) = \left(\frac{3 \cdot V_{WCW}}{2 \cdot L}\right)^{2/3} \cdot \left(\frac{g}{\eta}\right)^{1/3} \cdot (t - T_E)^{1/3} \tag{16}$$

The first derivative of Eq. [16] produces the wetting shock front velocity as

$$v(t)\big|_{z_W} = \left(\frac{V_{WCW}}{2 \cdot L}\right)^{2/3} \cdot \left(\frac{g}{3 \cdot \eta}\right)^{1/3} \cdot (t - T_E)^{-2/3} \tag{17}$$

Inserting $z_W(t)$ from Eq. [16] into Eq. [14] yields the mobile water content at the wetting shock front

$$w(t)\big|_{z_W} = \left(\frac{\eta}{g}\right)^{1/3} \cdot \left(\frac{3 \cdot V_{WCW}}{2}\right)^{1/3} \cdot (t - T_E)^{-1/3} \cdot L^{2/3} \tag{18}$$

while multiplication of Eq. [17] with Eq. [18] yields the volume flux density at the wetting shock front

$$q(t)\big|_{z_W} = \frac{V_{WCW}}{2 \cdot (t - T_E)} \tag{19}$$

Figure 2 illustrates the early part of a *WCW*.

Preprints (www.preprints.org) | NOT PEER-REVIEWED | Posted: 13 November 2019 doi:10.20944/preprints201911.0150.v1

Peer-reviewed version available at Water 2020, 12, 337; doi:10.3390/w12020337

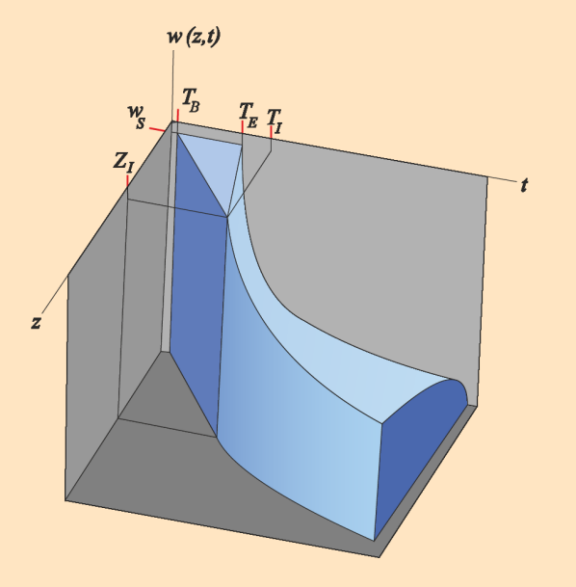

Figure 2: Schematic representation of a water-content wave *WCW,* where the *w(z,t)*-axis represents the mobile water content, *t* and *z* are the axes of time and depth; w_S indicates the mobile water content that follows from q_S; T_B and T_E (s) are the beginning and ending times of the water pulse $P(q_S, T_B, T_E)$ that hits the surface at $z = 0$; T_I and Z_I indicate time and depth of the wetting front intercepting the draining front. The wetting shock front continues beyond $t > T_I$ and $z > Z_I$ as curve along time and depth. (From Germann, 2014; with permission from the publisher).

A *WCW* easily translates into volume flux density according to

$$q(z,t) = b \cdot w(z,t)^3 \tag{20}$$

with $b = g/(3 \cdot L^2 \cdot \eta)$. The approach applies to laminar flow as assessed with the Reynolds number

$$Re = \frac{F \cdot v}{\eta} = \frac{F^3 \cdot g}{3 \cdot \eta^2} = \left(\frac{3 \cdot v^3}{g \cdot \eta}\right)^{1/2} \tag{21}$$

$Re \leq 1$ strictly defines laminar flow; however, depending on the application, $Re > 1$ might be tolerable, yet within an undisclosed range.

The following paragraph *b)* provides cuts of the *WCW* in the *z*-*w*(*z*,*t*)-plane of Fig. 2 while paragraph *c)* introduces cuts in the *t*-*w*(*z*,*t*)-plane.

b) Variation of a WCW with depth

The following inspects the spatial variation $w(z,\tau)$ of the *WCW*'s mobile water content during the three intervals of (i) $T_B \le \tau_1 \le T_E$, (ii) $T_E \le \tau_2 \le T_I$, and (iii) $T_I \le \tau_3 < \infty$.

(i) $T_B \le \tau_1 \le T_E$: Position of the wetting shock front, mobile water content, and volume flux density are

$$z_W(\tau_1) = \frac{g}{3 \cdot \eta} \cdot F^2 \cdot (\tau_1 - T_B) \tag{22}$$

$$w(z,\tau_1) = L \cdot F \tag{23}$$

$$q(z,\tau_1) = \frac{g}{3 \cdot \eta} \cdot F^3 \cdot L \tag{24}$$

Thus, piston flow occurs during infiltration, $T_B \le \tau_1 \le T_E$.

(ii) $T_E \le \tau_2 \le T_I$: The position of the wetting shock front is the same as in Eq.[22] while that of the draining front follows from Eq.[9] as

$$z_D(\tau_2) = \frac{g}{\eta} \cdot F^2 \cdot (\tau_2 - T_E) \tag{25}$$

Between $0 \le z \le z_D(\tau_2)$ the trailing wave evolves according to Eq.[14] as

$$w(z,\tau_2) = L \cdot \left(\frac{\eta}{g}\right)^{1/2} \cdot z^{1/2} (\tau_2 - T_E)^{-1/2} \tag{26}$$

The mobile water content remains constant at *w* between $z_D(\tau_2) \le z \le z_W(\tau_2)$ according to Eq.[23], and piston flow prevails according to Eq.[24].

(iii) $T_I \le \tau_3 < \infty$: Velocity, mobile water content, and volume flux density at the wetting shock front follow from Eqs.[17] to [19], while the profile $w(z,\tau_3)$ follows from Eq.[26].

Figure 3 illustrates the profiles of mobile water content at four typical times.

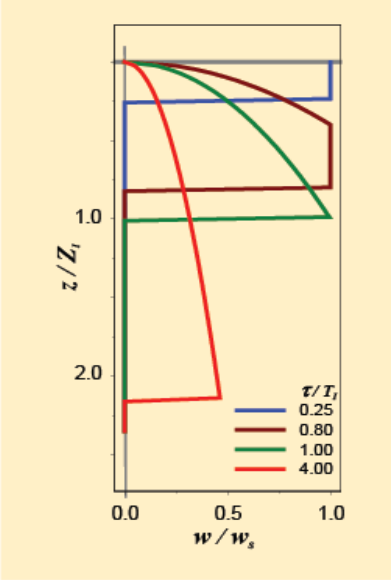

Figure 3: Profiles of relative mobile water content w/w_S as functions of relative depth z/Z_I at four relative times τ/T_I. (From Germann, 2014; with permission from the publisher).

c) Variation of a WCW with time

The following inspects the time series of a *WCW*'s mobile water content $w(\zeta,t)$ at the three depth ranges of (i) $0 \le \zeta_1 < Z_I$, (ii) $\zeta_2 = Z_I$, and (iii) $\zeta_3 \ge Z_I$.

(i) $0 \le \zeta_1 < Z_I$: The arrival times of the wetting shock and draining fronts at ζ_1 are

$$t_W(\zeta_1) = T_B + \frac{3 \cdot \eta}{g} \cdot F^{-2} \cdot \zeta_1 \tag{27}$$

$$t_D(\zeta_1) = T_E + \frac{\eta}{g} \cdot F^{-2} \cdot \zeta_1, \tag{28}$$

while the mobile water content assumes the following values during the respective time intervals:

$$T_B \le t \le t_W(\zeta_1): \qquad w(\zeta_1,t) = 0 \tag{29}$$

$$t_W(\zeta_1) \le t \le t_D(\zeta_1): \qquad w(\zeta_1,t) = L \cdot F \tag{30}$$

$$t \ge t_D(\zeta_1): \qquad w(\zeta_1,t) = L \cdot F \cdot \left(\frac{t_D(\zeta_1) - T_E}{t - T_E} \right)^{1/2} \tag{31}$$

Equation [31] results from solving Eq.[26] for ζ_1, and substituting with it the depth z in Eq.[24]. The equation represents the trailing wave.

Preprints (www.preprints.org) | NOT PEER-REVIEWED | Posted: 13 November 2019 doi:10.20944/preprints201911.0150.v1

Peer-reviewed version available at Water 2020, 12, 337; doi:10.3390/w12020337

(ii) $\zeta_2 = Z_I$: At depth of front interception and after $t \geq T_I$ the mobile water content becomes

$$w(\zeta_2, t) = L \cdot F \cdot \left(\frac{T_E - T_B}{2 \cdot (t - T_E)} \right)^{1/2} \tag{32}$$

Equation [32] results from replacing $t_D(\zeta_1)$ in Eq.[31] with T_I, Eq.[10].

(iii) $\zeta_3 \geq Z_I$: Solving Eq.[15] for t yields the arrival time of the wetting shock front at ζ_3 as

$$t_W(\zeta_3) = T_E + \frac{4}{9} \cdot \frac{\eta}{g} \cdot \left(\frac{L}{V_{WCW}} \right)^2 \cdot \zeta_3^3 \tag{33}$$

Inserting Eq.[33] into Eq. [14] yields the mobile water content at the crest as

$$w(\zeta_3) = \frac{3}{2} \cdot V_{WCW} \cdot \frac{1}{\zeta_3} \tag{34}$$

and the mobile water content as a function of time becomes

$$0 \leq t \leq t_W(\zeta_3) \qquad w(\zeta_3, t) = 0 \tag{35}$$

$$t \geq t_W(\zeta_3) \qquad w(\zeta_3, t) = \frac{3}{2} \cdot V_{WCW} \cdot \frac{1}{\zeta_3} \cdot \left(\frac{t_W(\zeta_3) - T_E}{t - T_E} \right)^{1/2} \tag{36}$$

Figure 4 illustrates four time series of $w(\zeta_i,t)$ at four different relative depths $[\zeta_i/Z_I]$.

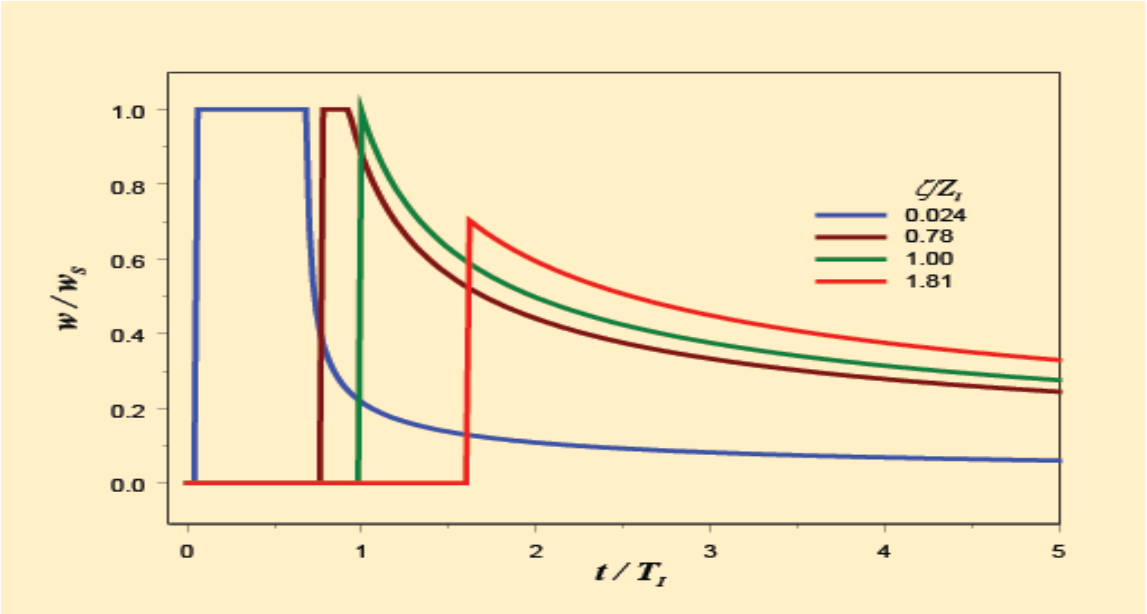

Preprints (www.preprints.org) | NOT PEER-REVIEWED | Posted: 13 November 2019 doi:10.20944/preprints201911.0150.v1

Peer-reviewed version available at Water 2020, 12, 337; doi:10.3390/w12020337

Figure 4: Time series of relative mobile water content, w/w_S as functions of relative time t/T_l at four relative depths ζ / Z_l. (From Germann, 2014; with permission from the publisher).

d) Routing pulse series

From mass balance requirement follows the celerity of an abrupt pulse increase from P_1 to P_2 with $q_2 > q_1$ and $w_2 > w_1$, as

$$c_j = \frac{q_2 - q_1}{w_2 - w_1} \tag{37}$$

Germann (2018c) provides the details of applying the theory and the method of characteristics to series of pulses.

The following section provides experimental support to the four presumptions. The next section presents various applications of Newton's shear flow approach to infiltration and drainage.

Experimental support for the four presumptions

This section experimentally supports the four presumptions that provide the base for Eqs. [1 to 36]: (i) infiltrating water forms a sharp wetting shock front; (ii) the wetting shock front moves with constant v; (iii) atmospheric pressure prevails in the *WCW*; and (iv) flow is laminar (i.e., Reynolds numbers close to 1). An infiltration experiment in the Kiel Sand Tank (alHagrey et al., 1999) produced the data that support presumptions (i) to (iv).

a) The Kiel Sand Tank

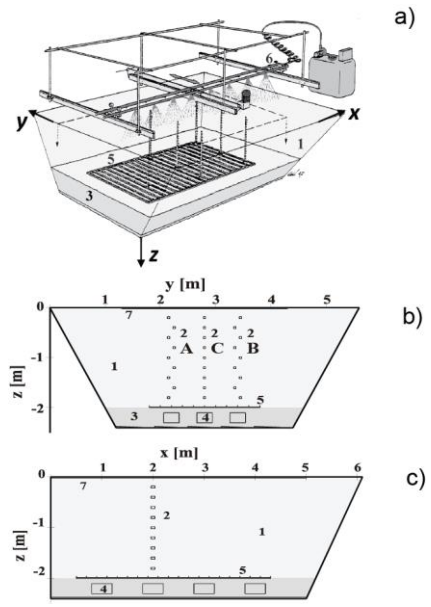

Figure 5: Overview of the experimental set-up of the full-scale model in (a) block diagram, (b) sections *yz* at *x* = 2(m), and (c) *xz* at *y* = 2.8(m). (1) sand, (2) tensiometers, TDR sensors (profiles A, B, C), (3) filtered-gravel horizon, (4) bottom drain, (5) GPR-electrode grid, (6) irrigation system, (7) surface profile of electrodes or radar antenna. (From Germann, 2014; with permission from the publisher).

The Kiel Sand Tank (alHagrey et al., 1999), Fig. 5, consists of a concrete vessel, 2 m deep, 3 m wide and 5 m long at the top. The tank was uniformly filled with sand in the texture range of 63 to 630 µm with particle and bulk densities of 2.8 and 1.5 (Mg m^{-3}), respectively, and hydraulic conductivity at saturation of K_{sat} = 1.3 x 10^{-4} (m s^{-1}). The system was equipped with a rain simulator, 9 TDR-probes and 18 tensiometers at 0.2 (m) vertical intervals, 2 GPR grids, and a drain system attached to a flow recorder. The experiment producing the data referred in here started on 9 June 1997 at 12:50 h. The freshly filled sand was sprinkled at with the rate q_S = 4.3 x 10^{-6} (m s^{-1}) (i.e., q_S/K_{sat}= 1:34) during (T_E-T_B) = 58620 (s) that was 720 (s) after the beginning of drainage flow. The total volumes of sprinkling and drainage, V_S and V_D, were 0.254 and 0.175 (m^3), respectively (i.e., V_D/V_S = 0.69).

Preprints (www.preprints.org) | NOT PEER-REVIEWED | Posted: 13 November 2019 doi:10.20944/preprints201911.0150.v1

Peer-reviewed version available at Water 2020, 12, 337; doi:10.3390/w12020337

b) Sharp wetting shock fronts: presumption (i)

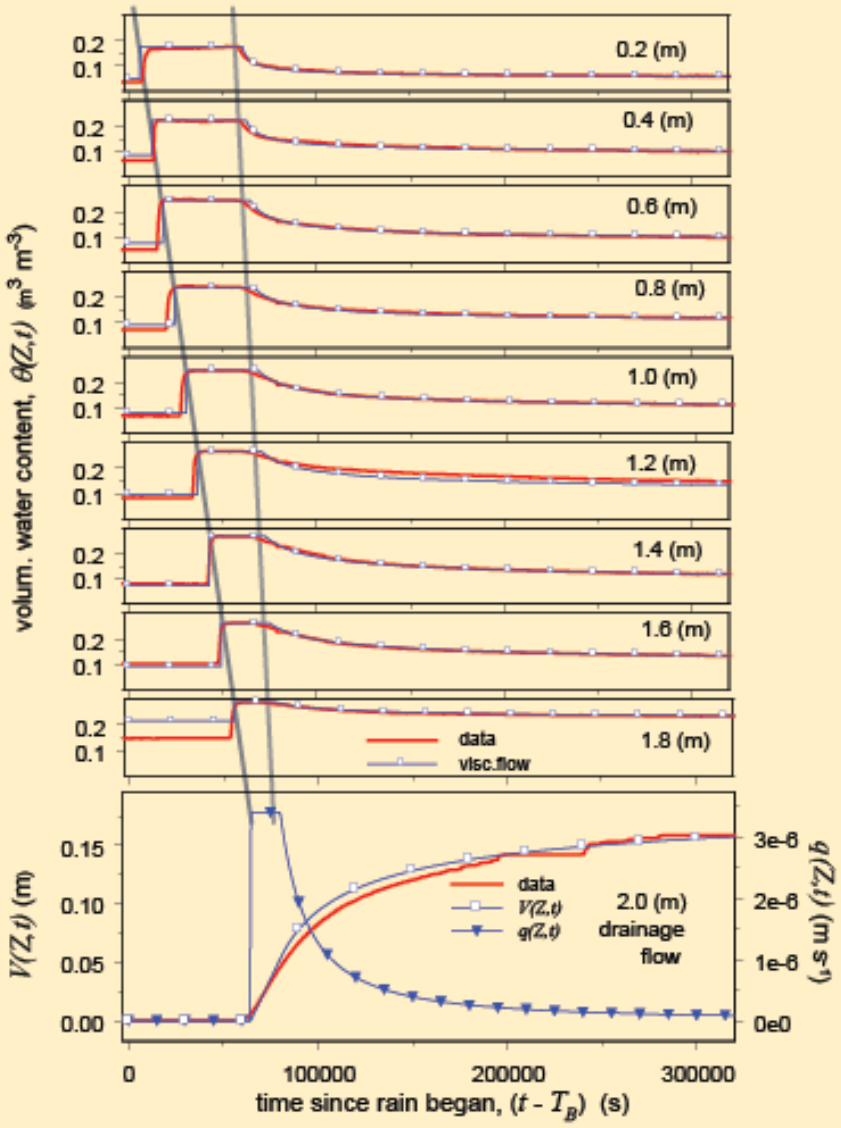

Figure 6: Time series of TDR-water contents $\theta(Z_j, t)$ (m^3m^{-3}) at nine depths and cumulative drainage $V(Z,t)$(m) in the Kiel-sand tank. The blue lines with square symbols illustrate shear-flow matching to the data. The volume flux density $q(Z,t) = dV(Z,t)/dt$ of drainage follows from the first derivative of $V(Z,t)$, Eq.[37], depicted in the lowest panel by the blue line with the triangles. The two gray lines across depth suggest constant velocities of the wetting shock and draining fronts, Fig.7. (From Germann, 2014; with permission from the publisher).

Preprints (www.preprints.org) | NOT PEER-REVIEWED | Posted: 13 November 2019 doi:10.20944/preprints201911.0150.v1

Peer-reviewed version available at Water 2020, 12, 337; doi:10.3390/w12020337

Figure 6 shows the evolution of $\theta(Z_j,t)$ during ($T_B \leq t \leq T_E$) at depths Z_j = 0.2, 0.4, 0.6, 0.8, 1.0, 1.2, 1.4, 1.6, and 1.8 (m). Sharp wetting shock fronts evolved at each depth across the tank, despite the low sprinkling rate compared with K_{sat}.

c) Constant velocity of the wetting shock front : presumption (ii)

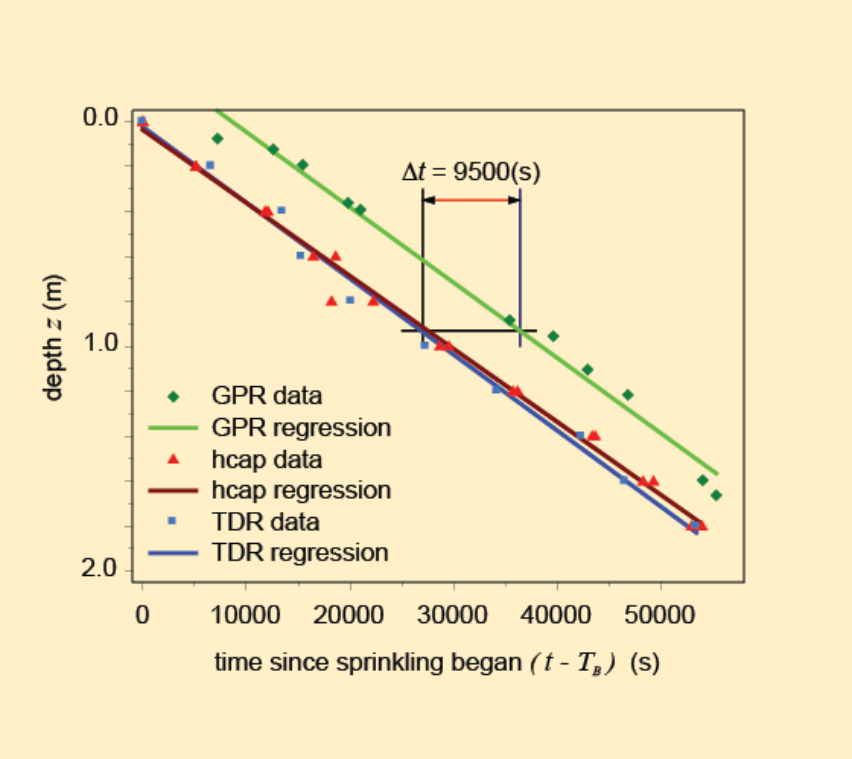

Figure 7*:* Regressions of depth vs. time of first recorded water content increases based on GPR-, tensiometer-, and TDR-data. Wetting front velocities are $v_W = dz_W/dt$ (m s^{-1}). The delay between the regressions of TDR- and tensiometer-readings versus GPR-readings amounts to [Δt = 9‘500(s)]. (From Germann, 2014; with permission from the publisher).

Figure 7 demonstrates the advancement of the wetting shock front with constant velocity $v_{W,1} = Z_j/t_W(Zj) = 3.2 \times 10^{-5}$ (m s^{-1}), derived from the tensiometer- and TDR-data, and of $v_{W,2} = 3.3 \times 10^{-5}$ (m s^{-1}), derived from the GPR-data. The coefficients of determination of the

Preprints (www.preprints.org) | NOT PEER-REVIEWED | Posted: 13 November 2019 doi:10.20944/preprints201911.0150.v1

Peer-reviewed version available at Water 2020, 12, 337; doi:10.3390/w12020337

two linear regressions of wetting shock front depths vs. arrival times resulted in $r^2 > 0.98$. The delay of the GPR-readings of 9500 (s) with respect to the tensiometer- and TDR-data still awaits an explanation.

d) Atmospheric pressure within the WCW: presumption (iii).

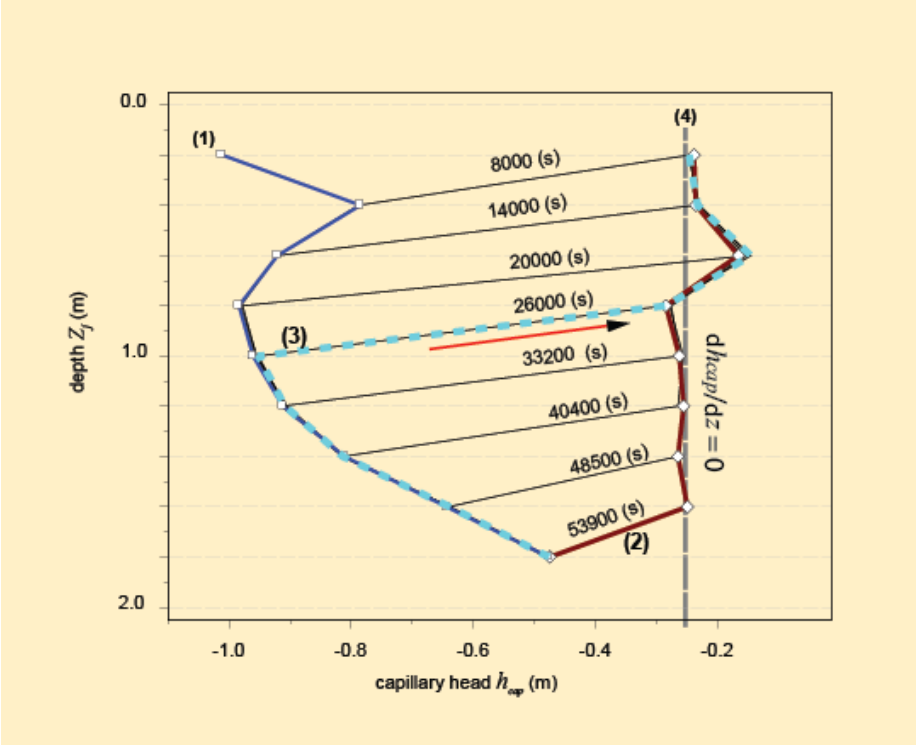

Figure 8: Profiles of capillary heads, $h_{cap}(z,T_k)$ at times T_k = 8‘000, 14‘000, 20‘000, 26‘000, 33‘200, 40‘400, 48‘500, 53‘900(s).

Profile (1), solid blue line: $h_{cap,init} = h_{cap}(\theta)$ at $t < T_B$;

Profile (2), solid red line: $h_{cap}(z)$ at t = 53‘900(s);

Profile (3), cyan dashed line: $h_{cap}(z)$ at t = 26‘000(s). The arrow points in the direction of back snapping of h_{cap} during the passing of the wetting shock front.

Profile (4), vertical gray dashed line, indicates $dh_{cap}/dz = 0$ at $h_{cap}(w)$ = -0.25(m).

(From Germann, 2014; with permission from the publisher).

Figure 8 illustrates the sudden increase of the capillary head h_{cap} (= ψ x ρ x g) from antecedent values of $-1.0 \leq h \leq -0.4$ (m) to close to atmospheric pressure at about -0.25 (m). Moreover,

Preprints (www.preprints.org) | NOT PEER-REVIEWED | Posted: 13 November 2019 doi:10.20944/preprints201911.0150.v1

Peer-reviewed version available at Water 2020, 12, 337; doi:10.3390/w12020337

with the exception of the depth range from 0.2 to 1.0 (m), the original gradient $dh_{cap}/d_z \approx -1$ snapped back to $dh_{cap}/d_z \approx 0$. Both sudden reactions of the capillary head on the passing of the wetting shock front indicate pressure close to atmospheric in the *WCW*. Likewise, based on measurements of acoustic velocities across a column of a partially water saturated soil during infiltration (Flammer et al., 2001), Germann (2018a) concluded that atmospheric pressure prevails in the *WCW* between the wetting shock front and the soil surface at least during $T_B \leq t \leq T_I$.

e) Laminar flow, Reynolds number: presumption (iv)

From the application of Eq. [21] to $v = 3x10^{-5}$ (m s^{-1}) follows $Re \approx 10^{-4}$ i.e., laminar flow. From more than 200 infiltration experiments, Hincapié and Germann (2009) reported a range of $10^{-5} < v < 2 \times 10^{-2}$ (m s^{-1}) leading to a range of $10^{-4} < Re < 1.6$. The upper limit is still considered to represent laminar flow. However, *Re* needs a closer look when applying Newton's shear flow, in particular to fissured rock formations.

Discussion

a) Coherence of the approach

The parameters *F* and *L* suffice to treat infiltration and drainage with Newton's shear flow approach, Eqs. [1] to [20]. In principle, time series of either $\theta(Z,t)$ or $q(Z,t)$ prmits calibration of the two parameters. Both procedures are introduced, using the data presented in Fig. 6.

F and L from θ(Z,t)-series: The observed arrival times $t_W(Z_j)$ of the wetting shock front at the nine depths Z_j led to $v_W = 3.25 \times 10^{-5}$ (m s^{-1}). From v_W follows *F* according to Eq. [8]. Together with *F*, Eq. [6] produces $L(w)$ from the amplitude $w_{max}(z) = (\theta_{max} - \theta_{end})$, where θ_{max} and θ_{end} refer to the maximum and end water contents of the measured time series $\theta(Z,t)$. The nine $\theta(Z,t)$-series yielding the range of $2.3 \times 10^4 \leq L(w) \leq 6.1 \times 10^4$ (m^2m^{-3}). See Germann (2018b) for details of parameter estimation from the *w*-version of Newton's shear flow.

F and L from q(Z,t)-series: Recording time-variable flow rates is frequently tagged with considerable noise due to the uncertainty of properly assigning the time to the collected volume fractions. The time integral of collected flow, however, circumvents the uncertainty. For instance, the bottom panel in Fig. 6 provides the continuously recorded sum of drainage from the Kiel Sand Tank as smooth curve well suited for calibrating $L(q)$. The theoretical counterpart of time-integrated flow follows from adding Eq. [30] and Eq. [31] under consideration of Eq. [20], and integrating the resulting expression from $t_W(Z)$ to $t > t_D(Z)$, yielding

$$V(Z,t) = F^3 \cdot L(q) \cdot \frac{g}{3 \cdot \eta} \cdot \left(3 \cdot t_D - 2 \cdot T_E - t_W - 2 \cdot \frac{(t_D - T_E)^{3/2}}{(t - T_E)^{1/2}} \right) \quad (37)$$

where Z refers to the depth of drainage flow at 2.0 (m). The specific contact area is the only factor left for matching Eq. [37] to the data that resulted in $L(q) = 3.3 \times 10^4$ ($m^2 m^{-3}$), comfortably lying within the range of $L(w)$. This demonstrates the coherence of Newton's shear flow approach to infiltration and drainage.

b) Scale tolerance

Dubois (1991) injected the tracers uranin and eosin about 1800 (m) above the Mont Blanc car tunnel that connects Chamonix (France) with Courmayeur (Italy). Within 108 (d) he detected the tracer fronts in seeps in the car tunnel. This amounts to $v_W \approx 2 \times 10^{-4}$ ($m\ s^{-1}$), that is about seven times faster than v_W in the sand tank, yet well within the range of the v_W-collection reported above.

Hincapié and Germann (2010) investigated with neutron radiography the water content variations during finger flow in sand boxes with the dimensions of height, width and thickness of 400, 200, and 50 (mm), respectively. The boxes were filled with quartz sand sieved to particle diameters from 0.2 to 0.5 (mm). Voxel dimensions were 0.27 (mm) x 0.27 (mm) x 50 (mm). Water balance calculations were based on flux estimations in layers of height and width of 1 and 30 pixels, respectively. The layers were positioned within observed fingers at the

depths of 100, 150, and 200 (mm). Fluxes in each layer followed from Newton's shear flow approach. The flux differences from layer to layer deviated utmost by 19% from the corresponding water content changes in the volumes between the layers (Germann, 2014).

Dubois' (1991) observations across 1800 (m) of crystalline rocks of the Mont Blanc massif and the water balance calculations of finger flow in the sand box of Hincapié and Germann (2010) at the scale of millimeters hint at the spatio-temporal tolerance of Newton's shear flow that may advance the approach to an attractive tool, for instance, for the study of infiltration into groundwater systems.

c) Preferential and retarded tracer breakthrough

Preferential flow in soil hydrology is frequently associated with enhanced and accelerated solute and pollutant breakthrough (e.g., Larsbo et al., 2014). However, Bogner and Germann (2019) reported considerable delays of tracer breakthrough compared with the first arrival of the wetting shock fronts at the bottoms of soil columns with heights of 0.4 (m). They referred to the phenomenon as 'pushing out old water' that is well known in catchment hydrology. They statistically explained 81% of the observed delay variations with combinations of L and F when applying Newton's shear flow to the data. Tracer exchange on large L from thin F of the *WCW* may be even faster than presumed 'preferential' tracer transport. Under consideration of the mechanistic parameters F and L, Newton's shear flow provides for a novel tool for the unambiguous investigation of tracer transport and exchange i.e., accelerated as well as decelerated breakthrough.

d) Gravity vs. capillarity

Schumacher (1864) suggested a two-process approach to water flow and storage in partially saturated permeable media. While he recognized capillarity as responsible for the water's rise, and probably also its contribution to water redistribution in soil columns, he left open the

mechanism behind infiltration. This paper concentrates on infiltration that is completely gravity-driven and viscosity-controlled, yet allowing for water abstraction due to capillarity from the mobile to the immobile part of the permeable system. Concentrating on gravity and viscosity liberates infiltration and drainage from the omnipresence of capillarity in soil hydrology with the benefit of avoiding the difficult definitions of non-equilibrium flow and the separation of macropores from the remaining pores. With respect to capillarity, the relative contribution of gravity to flow varies according to $cos(\alpha)$, where α (°) is the angle of deviation from the vertical. Thus, at $cos(0°) = 1$, as in the cases presented above, gravity's contribution is at maximum; it reduces to $cos(90°) = cos(270°) = 0$, while it completely opposes capillarity at $cos(180°) = -1$.

e) Shear flow and Darcy's law

Darcy's (1856) law mutates to an extension of unsaturated vertical shear flow. From Eq. [5] follows:

$$\theta_{ante} + w < \varepsilon \text{ and } \Delta p/\Delta z = \rho\, g: \qquad q = \frac{F^3 \cdot L}{3 \cdot \mu} \cdot \rho \cdot g \qquad [38]$$

where θ_{ante} (m^3m^{-3}) is the antecedent volumetric water content, ε (m^3m^{-3}) is porosity, $\Delta p/\Delta z$ (Pa m^{-1}) is the pressure gradient, ρ (=1000 kg m^{-3}) is the density of water, and $\mu = \rho\, \eta$ (Pa s) is dynamic viscosity. At saturation we get:

$$\theta_{ante} + w = \varepsilon \text{ and } \Delta p/\Delta z = \rho\, g: \qquad q_{sat} = \frac{F_{sat}^{\ 3} \cdot L_{sat}}{3 \cdot \mu} \cdot \rho \cdot g = K_{sat} \qquad [39]$$

while an external pressure gradient leads to :

$$\theta_{ante} + w = \varepsilon \text{ and } \Delta p/\Delta z > \rho \text{ x } g: \qquad q(p) = \frac{F_{sat}^{\ 3} \cdot L_{sat}}{3 \cdot \mu} \cdot \frac{\Delta p}{\Delta z} = q_{sat} \cdot \frac{\Delta p}{\Delta z \cdot \rho \cdot g} \qquad [40]$$

Darcy's law states that $q \propto \Delta p/\Delta z$ i.e., volume flux density is a linear function of the flow-driving gradient with the proportionality factor K_{sat}. In view of the various dimensionalities of

Preprints (www.preprints.org) | NOT PEER-REVIEWED | Posted: 13 November 2019 doi:10.20944/preprints201911.0150.v1

Peer-reviewed version available at Water 2020, 12, 337; doi:10.3390/w12020337

$w \propto (L^1,F^1)$, $v \propto (L^0, F^2)$, and $q \propto (L^1, F^3)$, linearity seems only possible if F_{sat} and L_{sat} remain constant and independent from p in the transition from gravity-driven to pressure-driven shear flow at saturation i.e., in the transition from Eq. [38] to Eq. [40]. This elaboration supports the linearity of Darcy's law, but it is not its independent proof. As a consequence, $w = q/v$ also remains constant. Further, if $\theta_{ante} + w = \varepsilon$, $dL_{sat}/dp = 0$ and $dF_{sat}/dp = 0$ then follows the hypothesis that (F_{sat} x L_{sat}) represent $(F\ x\ L)_{max}$ leading to K_{sat}. However, other combinations of ($F\ x\ L$) in unsaturated media are feasible that may lead to $q > q_{sat} = K_{sat}$. This unproven speculation opens an unexpected view on shear flow, that is in stark contrast to Richards (1931) capillary flow, where a priori $K_{sat} > K(\theta$ or $\psi)$. See Germann and Karlen (2016) for further discussion.

f) Water abstraction from the WCW

Pressure in the *WCW* is atmospheric while $\psi < 0$ typically prevails ahead of it. Therefore, water is abstracted from the *WCW* onto *L*. Abstraction is usually completed during short periods as the $\theta(Z,t)$-series in Fig. 6 demonstrate. The amount of abstraction shows in the difference between θ_{end} and θ_{ante}.

Conclusions

Newton's shear flow provides for a cohesive approach to infiltration and drainage in permeable media, and no a priori decisions on pore properties are required. So far, the approach is in its descriptive mode, capable of quantifying infiltration and drainage with the two parameters film thickness *F* and specific contact area *L*. However, the analytical expressions facilitate the development of predictive model applications such as to groundwater recharge and to the transport of solutes and particles. Advances are expected from research, among other topics, in

the relationships of F and L with antecedent soil moisture, intensity of infiltration, and hydraulic conductivity K_{sat}.

Finally, Newton's shear flow seems to have solved the 7th Unsolved Problem in Hydrology (Blöschl et al., 2019) that asks "Why is most flow preferential across multiple scales and how does such behaviour co-evolve with the critical zone?". However, Newton's shear flow as the solution of the 7th UPH did not evolve from the suggested dual-porosity perspective but from a hydro-mechanical point of view that does neither require preferential flow nor co-evolution of flow paths.

Acknowledgment

I thank Dr. Scholle, Guest Editor of the Special Issue on "Physical and Mathematical Fluid Mechanics", for inviting the manuscript to WATER.

References

Abou Najm, M.R. et al. 2019. Editorial: The uniformity of non-uniform flow across scales, processes and applications. Vadose Zone J. in process.

al Hagrey, S.A., T. Schubert-Klempnauer, D. Wachsmuth, J. Michaelsen, and R. Meissner. 1999. Preferential flow: First results of a full-scale flow model. Geophys. J. Int. 138:643–654.

Atalah, N.M., and M. R. Abou Najm. 2018. Characterization of synthetic porous media using non-Newtonian fluids: experimental evidence. Europ. J. of Soil Sci. 2018. Doi: 10.1111/ejss.12746

Beven, K. 2018. A century of denial: Preferential and nonequilibrium water flow in soils, 1864 - 1984. Vadose Zone J. 17:180153. Doi:10.2136/vzj2018.08.0153

Beven, K., and P. Germann. 1981. Water flow in soil macropores. II. A combined flow model. J. of Soil Sci.(British) 32: 15-29.

Beven, K., and P. Germann. 1982. Macropores and water flow in soils, Water Resour. Res., 18(5), 1311-1325**.**

Blöschl, G. et al. 2019. Twenty-three Unsolved Problems in Hydrology (UPH) – a community perspective. Hydrological Sciences Journal, 64, pp. 1141-1158, doi: 0.1080/02626667.2019.1620507.

Bogner, C., and P. Germann. 2019. Viscous flow approach to "pushing out old water" from undisturbed and repacked soil columns. Vadose Zone J. 18:180168. Doi: 10.2136/vzj2018.09.0168.

Buckingham, E. 1907. Studies on the movement of soil moisture. Bulletin 38. U.S. Department of Agriculture, Bureau of Soils, Washingron D.C.,

Burger, H. 1922. Physikalische Eigenschaften von Wald- und Freilandböden. Mitteilungen der schweizerischen Centralanstalt für das forstliche Versuchswesen XIII, 1-11.

Darcy, H. 1856. Les fontaines publiques de la ville de Dijon. Dalmont, Paris

Dubois, J.-D. 1991. Typologie des aquifers du cristallin: Exemples des massifs des Aiguilles Rouges et du Mont-Blanc. (Typology of Aquifers in the Cristaline: Examples from the Massifs Aguilles Rouges and Mt. Blanc). Ph.D.-dissertation 950. Department of Civil Engineering, EPFL, Lausanne (Switzerland). **9, 13**

Dupuit, J. 1863. Études théoriques et pratiques sur le movement des eaux dans les canaux découverts et à travers les terrains perméable. 2 me Ed. Paris: Dunod.

Flammer, I., A. Blum, A. Leiser, and P. Germann. 2001 Acoustic assessment of flow patterns in unsaturated soil. *J. of Applied Geophys*. 46**:**115-128. **12**

Fourier, J.B.J. 1822.Théorie analytique de la chaleur. F. Didot, Paris

Gardner, W., O.W. Israelsen, N.E. Edlefsen, and H. Clyde.1922. The capillary potential function and its relation to irrigation practice. Phys. Rev. 20, 196

Germann, P. 1985.Kinematic wave approach to infiltration and drainage into and from soil macropores. Trans. ASAE, 28(3): 745-749.

Germann, P. 1986. Rapid drainage response to precipitation. Hydrol. Proc. 1: 3-13.

Germann, 2014. Preferential Flow - Stokes Approach to Infiltration and Drainage. Geographica Bernensia, Bern (Switzerland), 199 p.

Open Access File under: https://boris.unibe.ch/119081/1/preferential_flow.pdf.

Germann, P. 2017. Comment on "Understanding preferential flow in the vadose zone: Recent advances and future prospects" by N. Jarvis et al. Vadose Zone J. 16(5). Doi: 10.2136/vzj2017.01.0004c.

Germann, P. 2018a. Viscosity-the weak link between Darcy's law and Richards' capillary flow. Hydrol. Proc. 32: 1166-1172. Doi:10.1002/hyp.11450.

Germann, P.2018b. Preferential flow at the Darcy scale: parameters from water content time series. Methods of Soil Analysis 2018, Vol. 3: 160121. Doi: 102136/msa2016.0121.

Germann, P. 2018c. Hydromechanics and kinematics in preferential flow. Soil Science 183(1):1-10. Doi:10.1097/SS.0000000000000226.

Germann, P., and K. Beven.1981a. Water flow in soil macropores. I. an experimental approach. J. of Soil Science (British) 82: 1-13.

Germann, P., and K. Beven.1981b. Water flow in soil macropores. III. A statistical approach. J. of Soil Science (British) 82: 31-39.

Germann, P., and M. Karlen. 2016. Viscous-flow approach to in situ infiltration and in vitro saturated hydraulic conductivity determination. Vadose Zone J. 15 (2).

Doi: 10.2136/vzj2015.05.0065

Hincapié, I., and P. Germann. 2009. Abstraction from infiltrating water content waves during weak viscous flows. Vadose Zone J. 8:996–1003; doi:10.2136/vzj2009.0012.

Hincapié, I., and P. Germann. 2010. Water content wave approach applied to neutron radiographs of finger flow. Vadose Zone J. 9:278-284; doi:10.2136/vzj2009.0102.

Jarvis, N., J. Koestel, and M. Larsbo. 2016. Understanding preferential flow in the vadose zone: Recent advances and future prospects. Vadose Zone J. 15(12). Doi 10.2136/vzj2016.09.0075.

Jarvis, N., J. Koestel, and M. Larsbo. 2017. Reply to 'Comment on "Understanding preferential flow in the vadose zone: Recent advances and futer porspects" by N. Jarvis et al.' Vadose Zone J. 16(5). Doi: 10.2136/vzj2017.01.0034r.

Larsbo, M., J. Koestel, and N. Jarvis. 2014. Relations between macropore network characteristics and the degree of preferential solute transport. Hydrol. Earth Syst. Sci., 18, 5255–5269, https://doi.org/10.5194/hess-18-5255-2014.

Lawes, J.B., J.H. Gilbert, and R. Warington. 1882. On the Amount and Composition of the Rain and Drainage Water Collected at Rothamsted. Williams, Clowes and Sons Ltd., London. 167 p.

Lighthill M.J., and G.B. Witham. 1955. On kinematic waves, I. Flood movement in long rivers. Proc. R. Soc. London, Ser. A, 229: 281-316.

Morbidelli, R., C. Corradini, C. Saltalippi, A. Flammini, J. Dari, and R.S. Govindaraju. 2018. Rainfall infiltration modelling. Water 2018, 10, 1873. Doi: 103390/w10121873

Newton, I. 1729. The Mathematical Principles of Natural Philosophy- Translation into English. Vol. II, p.184, Benjamin Motte, London (UK).

Ohm, G. S.1825. Vorläufige Anzeige des Gesetzes, nach welchem Metalle die Contact-eletricität leiten. In: J.C. Poggendorff (Hrsg.) : Annalen der Physik und Chemie. Berlin, Bd. 80, S. 79-88.

Or, D. 2018. The tyranny of small scales on presenting soil processes in global land surface models. Doi:10.1029/2019WR024846

Poiseuille, J.L.M. 1846. Recherches expérimentales sur le mouvement des liquides dans les tubes de très petits diamètres. Comptes Rendus, xi-xii. Mém. des Sav. Etrangers, ix. **2**

Richards, L.A. 1931. Capillary conduction of liquids through porous mediums. Physics 1:318-333

Richardson, L.F. 1922. Weather prediction by numerical process. Cambridge University Press: Cambrdige, UK.

Schumacher, W. 1864. Die Physik des Bodens. Wiegandt & Hempel, Berlin.

Simunek, J., M.T. van Genuchten, and M. Sejna. 2008. Development and applications of the HYDRUS and STANMOD software packages and related codes all rights reserve. Vadose Zone J. 7: 587-600. Doi: 10.2136/vzj2007.0077

van Genuchten, M. T.1980. A closed form equation for predicting hydraulic conductivity of unsaturated soils. Soil Sci. Soc. Am. J. 44: 892-898.

Veihmeyer, F.J. 1927. Some factors affecting the irrigation requirements of deciduous orchards. Hilgardia 2(6): 190 ff.

Veihmeyer, F.J. 1954. Soil moisture. In: Handbuch der Pflanzenphysiologie, Springer -Verlag, Heidelberg.

Young, T.1805. An essay on the cohesion of fluids. Philosophical Transactions of the Royal Society of London, The Royal Society, London. Vol. 95, p. 65-87